Geoenvironmental Disasters

RESEARCH

Open Access

Event-based landslide inventory through very high-resolution optical images and field surveys

P. Confuorto[1*], R. Franceschini[2], L. Scarpitta[1], N. Casagli[1,2], S. Morelli[3], F. Raspini[1], V. Tofani[1] and S. Moretti[1]

Abstract

Background Landslide inventories are essential tools for emergency response, hazard assessment, and susceptibility mapping, especially following very hazardous events. On 15 September 2022, an extreme rainfall event affected the Misa River basin in the Marche region, Central-Eastern Italy, resulting in widespread hydrogeomorphological instability, including numerous landslides and debris flows. Understanding the distribution and characteristics of these failures is vital for post-event analysis and future risk mitigation.

Objectives This study aims to develop a detailed post-event landslide inventory of the Misa basin and to analyze the spatial distribution, the main morphological features, and the environmental context of the triggered landslides. A further objective is to evaluate the impact of these landslides on the built environment, particularly roads and buildings.

Methods The landslide inventory was created using four Very High-Resolution (VHR) satellite imagery datasets (spatial resolution ranging from 3 m to 0.4 m), acquired before and after the event. Semi-automatic approaches, including NDVI (Normalized Difference Vegetation Index) change detection and segmentation/classification, were employed to assist visual photointerpretation. Field surveys were carried out to validate and refine the mapped landslides. Each landslide was classified according to its type of movement. Additional analyses included spatial density mapping, shape characterization using a roundness index, and correlation with geological, geomorphological, land cover, and rainfall data.

Results The final inventory comprises 805 landslides, categorized by movement type and spatially analyzed. The results highlight specific distribution patterns influenced by geomorphological and geological settings. A notable number of landslides affected infrastructure, with direct impacts recorded on both road networks and buildings. Morphometric analysis revealed variability in landslide shapes and sizes, reflecting diverse failure mechanisms triggered by the intense rainfall.

Conclusions This study provides new insights into the dynamics of landslides induced by extreme meteorological events, which are becoming increasingly frequent in Mediterranean regions. The event-based inventory not only supports a better understanding of triggering and preparatory factors but also contributes to improving emergency planning and future landslide susceptibility assessments in similar settings.

*Correspondence:
P. Confuorto
pierluigi.confuorto@unifi.it
[1] Earth Science Department, Università Degli Studi Di Firenze, Via La Pira 4, 50121 Florence, Italy
[2] OGS, Istituto Nazionale di Oceanografia e di Geofisica Sperimentale, Borgo Grotta Gigante, 42/C, 34010 Sgonico (Trieste), Italy
[3] Dipartimento di Scienze Pure e Applicate (DiSPeA), Università Degli studi di Urbino Carlo Bo, Via Ca' Le Suore, 2-4, Urbino, Italy

Springer Open

© The Author(s) 2025. **Open Access** This article is licensed under a Creative Commons Attribution 4.0 International License, which permits use, sharing, adaptation, distribution and reproduction in any medium or format, as long as you give appropriate credit to the original author(s) and the source, provide a link to the Creative Commons licence, and indicate if changes were made. The images or other third party material in this article are included in the article's Creative Commons licence, unless indicated otherwise in a credit line to the material. If material is not included in the article's Creative Commons licence and your intended use is not permitted by statutory regulation or exceeds the permitted use, you will need to obtain permission directly from the copyright holder. To view a copy of this licence, visit http://creativecommons.org/licenses/by/4.0/.

Introduction

Landslides in Italy are among the major threats in terms of economic damage and life loss due to the geological and morphological characteristics of the Italian territory, which is 75% mountainous-hilly with 1.3 million residents at direct risk (Trigila et al. 2021). They can be triggered by a variety of causes, either natural or anthropogenic However, especially in the last decade, rainfall-induced landslides are more widespread than any other geological event and occur anywhere in Italy, with serious consequences for people and property (Peruccacci et al. 2023). The current climate change scenario is exacerbating the occurrence of landslides on a global scale, with the Mediterranean region being particularly affected. In fact, more and more research are focusing on the impact, in terms of triggered landslides, of the so-called medicanes (Mediterranean tropical-like hurricanes) on the mediterranean areas (Valkianotis et al. 2022; Diakakis et al. 2023; Kushabaha et al. 2024). Scardino et al. (2024) found a relationship between the increase of Sea Surface Temperature and the occurrence of Medicanes, representing thus a potential proxy for geohazards correlated to such events. The latest climatic trend highlights a general reduction in the total rainfall while there is an increase in extreme rainfall event frequency (Donnini et al. 2023). Therefore, climate change, caused by global warming in recent years, is expected to lead to an increase in the rate of landslide phenomena in the near future (Gariano et al. 2018). To provide a prompt database of rainfall-induced impacts and consequences, which may be useful for reliable analysis, including susceptibility and risk assessment, the preparation of landslide inventories in the aftermath of extreme rainfall events assumes capital importance (Guzzetti et al. 2012; Smith et al. 2021a, b). The compilation of precise landslide inventories relies on several methods, spanning from traditional in-situ surveying (Pellicani et al. 2015; Lazzari et al. 2018) to the visual interpretation of aerial or satellite images (Hölbling et al. 2017; Del Soldato et al. 2018), with the support of Digital Elevation Models (DEMs, Lazzari et al. 2018; Pawluszek 2019) up to semi or automatic machine or deep learning-based algorithms using optical or radar satellite data (Plank et al. 2016; Mondini et al. 2019; Catani et al. 2021; Su et al. 2021; Meena et al. 2022). The latter can be used also to update landslide state of activity, through MultiTemporal SAR Interferometry (Bonì et al. 2024; Confuorto et al. 2023). In any case, recent technologies are drastically changing the way Earth Observation is deployed in landslide mapping (Novellino et al. 2024). According to a recent review (Novellino et al. 2024), in 40% of papers, landslide mapping was performed through change detection approaches (i.e. identification of changes that occurred between pre- and post-event imagery), while 9% used specific indexes (e.g., Normalised Difference Vegetation Index, NDVI), 6% segmentation, the grouping of pixels into shapes, while AI (Artificial Intelligence) works count 16%. The redaction of landslide inventories in the aftermath of extreme rainfall events is a consolidated practice: Mondini et al. 2011a, b tested semi-automatic approaches over a dataset of Very High Resolution optical multispectral imagery to detect shallow landslides triggered by a high-intensity rainfall in Messina province (Sicily, Italy); Ferrario and Livio 2024 presented an inventory of more than 47,000 landslides, redacted by visual interpretation, triggered by two main storms occurred in Emilia Romagna region (Italy) in May 2023. In Europe, extreme events that triggered shallow and/or rapid landslides are registered, for instance, in the Austrian Alps (Dietrich and Krautblatter 2017) or along the Pyrenees (Hürlimann et al. 2022), while also Typhoons and Hurricanes may lead to the clustered trigger of landslides, such as in the eastern coastal sector of China (Zeng et al. 2023) or in Puerto Rico (Ramos-Scharròn et al. 2020).

Here the landslide inventory of the Misa hydrographic basin (Ancona province, Eastern Central Italy) is presented. Misa basin is one of the river basins on the mountain side facing the Adriatic Sea that suffered an extreme rainfall event on September 15, 2022. Such an event lasted approximately 9 h and hit a large portion of the territory located between the Umbria and Marche border. In detail, the rain gauge of Cantiano village (Pesaro Urbino province) registered a peak intensity of 419 mm in the 9 h of rainfall, ca. 30% of the mean annual rainfall (Morelli et al. 2023). This extreme event caused erosion and a subsequent major flood along the Misa River, claiming the life of 12 people in its paroxysmal phase and causing extensive damage to structures and infrastructures. Furthermore, thousands of landslides were triggered by the abundant precipitations: Santangelo et al. 2023 reported 1687 landslides that were recognized through field activities; the area chosen include the territory with the highest rainfall intensity (Cantiano municipality area), for a total area of about 550 km^2, partially covering the Misa catchment area and including part of Metauro, Cesano and Esino basins, located westwards of Misa. In this work, a mixed approach, based on the integration of segmentation and supervised classification and visual interpretation of pre- and post-event VHR (Very High Resolution) imagery, allowed us to recognize more than 700 landslides in the Misa basin that were subsequently validated through field surveying. Differently from Santangelo et al. 2023, here the adoption of VHR imagery was necessary to provide a summary of the event in the framework of an agreement with Regional authorities, aimed at the implementation of new and updated susceptibility and

risk maps. Beyond the description of the landslide distribution, here we analyzed also the impact of such events on the urban setting of the territory and compared such inventory with past records belonging to official repositories. Such dataset and analyses have provided a base for implementing an event-based susceptibility assessment of the area to improve the Misa basin's territorial management (Caleca et al. 2024).

Study area and rainfall event

Geological and geomorphological setting

The Misa basin extends over an area of approximately 380 km^2, including 17 municipalities, all located in the Ancona province, Eastern Central Italy (Fig. 1a). The Misa River is 48 km long and flows into the Adriatic Sea at the city of Senigallia. The hydrographic network is clearly asymmetrical: the tributaries on the hydrographic left, more developed, mainly feed the water flow of the Misa River (Ilari 2020). Its main tributary is the Nevola River, having a parallel direction to the Misa River according to the distribution pattern of the main watercourses typical of central-eastern Italy due to the regional tectonic structure. The Nevola River flows its waters into the Misa River approximately 9 km from the entrance of the Misa River into the Adriatic Sea (Fig. 1a). Both has a marked torrential regime with impetuous flows in the rainy seasons, which generally occur in autumn and spring in these areas, and even though they are relatively small, they are capable of carrying a large amount of sediment towards the sea (Brocchini et al. 2017).

From the geological point of view the study area is located within the Umbria-Marche Apennines, precisely in the external Marche basin (Centamore et al. 1991). The main tectonic lines have NW–SE direction, as the structural setting of the Umbria-Marche Apennines (Centamore et al. 1986). The area can be distinguished into two separate sectors: on the western side, there is a mountainous-hilly landscape prevailing, with mainly calcareous and marly-calcareous outcrops; on the eastern flank, the landscape is mainly flat or gently hilly, with mainly pelitic and arenaceous-pelitic formations (Fig. 1b).

In detail, the mountainous area consists of a system of folds and faults in which cretaceous formations outcrop, such as Maiolica (Micarelli et al 1977) and Marne a Fucoidi, micritic limestones and clayey marls, respectively along with palaeogenic formations, among which the Scaglia bianca, rossa and variegata, and the Scaglia cinerea, limestones with chert nodules and marls-silty marls, respectively. The hill and the alluvial plain areas havemainly formations of the Plio-Pleistocene succession characterised by clays, marly clays, sandy-silty clays with sandstone intercalation and the Quaternary continental

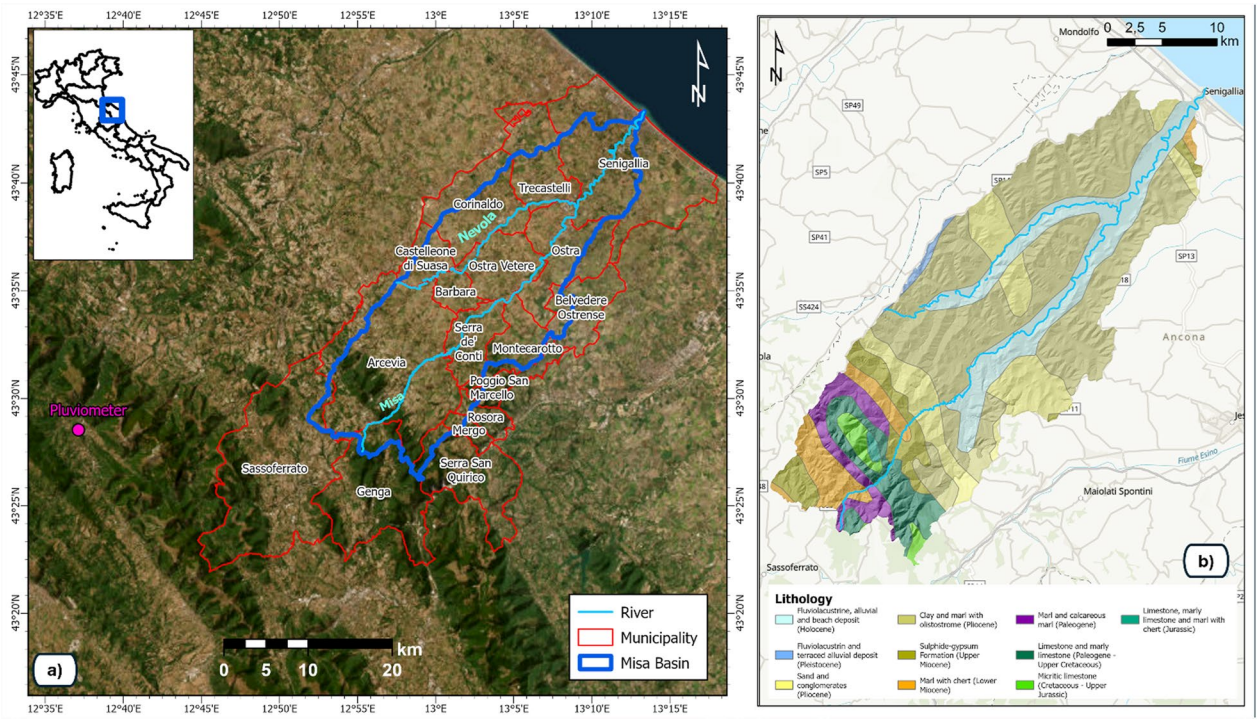

Fig. 1 **a** Setting of the study area and administrative division. In the inset, the location of the Misa basin within Italian territory; **b** Geolithological map of the Misa basin (derived from Geological Map of Italy 1:500,000 by ISPRA).

deposits constituting the alluvial terraces of the 1 st to 4th order outcrop (Fig. 1b).

Regarding the geological-structural evolution, morphostructures of Miocene origin have conditioned the morphology of the Misa River basin, and consequently also the network of watercourses present. The basin has a narrow and elongated shape along the direction of the anti-Apennine tectonic lines (SW—NE).Therefore, the course of the Nevola and Misa rivers may be due to a fluvial capture caused by neotectonic phenomena (Guerrera and Wezel 1979).

The rapid tectonic uplift that occurred between the Lower Pleistocene and Middle Pleistocene generated a durable valley deepening, developing narrow and deep V-shaped valleys in the mountainous part of the basin, while on the pelitic-arenaceous terrain, the valleys widen, and terraced alluvial deposits can be found on the slopes. Furthermore, in the westernmost part of the basin, where calcareous and marly limestone lithologies are present, the relief energy of the slopes is more accentuated; the high slopes consequently generate landslide phenomena, typically rockfalls and translational slides. In the other portions of the territory, the presence of pelitic and pelitic-arenaceous lithotypes considerably varies the geomechanical properties of the area, making it easily erodible despite the low slopes. The eluvial-colluvial coverings can be affected by instability, especially during intense rainfall, playing a fundamental role in triggering landslide phenomena such as flows, translational slides, river-bank landslides and shallow landslides. The land cover of the study area is also very indicative of a prevalent agricultural vocation of the territory, with mostly Corine Land Cover classes belonging to the 2nd group (Agricultural areas).

September 15, 2022 pluviometric event

The pluviometric event developed over Umbria and Marche, mainly affecting an area of about 5,000 km^2 in the provinces of Ancona and Pesaro-Urbino with considerable ground effects. The highest peak rainfall data was obtained from the Cantiano (PU) rain gauge (whose location can be found in Fig. 1a) and revealed a maximum rainfall intensity of 419 mm in 9 h, while within the Misa basin the maximum values were recorded in rain gauge of Colle (within Montecarotto territory, SE flank of the basin, 186 mm in 6 h and 204 mm in 12 h) located in the mountain sectors on the right hydrographic side (Morelli et al. 2023). This portion of the basin represents one of the areas of maximum rainfall intensity after that of Cantiano. The Marche Regional Functional Centre has reconstructed the path of the thunderstorm system triggered on the morning of September 15 in the area under analysis (Fig. 2). From the late morning of the 15th, several thunderstorm systems formed on the Tyrrhenian side of the peninsula, favored by the presence of humidity provided by the Tyrrhenian Sea and the orographic effects of Sardinia and Corsica and then Tuscany, as the system migrated eastwards. During this time other storm cells were generated, first involving Tuscany and Umbria and then extending towards the Marche. In the first phase, the phenomena affected the central-northern mountainous and high-hill areas of the region, decreasing in intensity moving toward the coast (Morelli et al. 2023). In the late afternoon, a self-regenerating and stationary system formed from the western side, which affected not only the inland areas of Marche and Umbria but also the hilly and coastal part of the province of Ancona, bringing high amounts of precipitation in a very short time and causing widespread criticality in the Candigliano, Cesano, Misa and Sentino basins. This led to an increase in rainfall intensity and extended its area of interest also to the hilly and coastal areas of the province of Ancona. From 5 p.m. local time until 8 p.m., the system was intense and stationary, generating accumulations that locally exceeded 400 mm.

Data and methods

Data

In order to draw up an event-based inventory of landslides, very high-resolution multispectral optical satellite images were acquired, both pre-event, to set up a baseline scenario, and post-event, to verify the changed ground conditions following the rainfall (Table 1). For the mapping of the landslides triggered on September 15, 2022, 4 multispectral optical satellite datasets were acquired: in detail, 2 SPOT-6 images, acquired on April 30, 2022, 2 WorldView-2 images, acquired on May 22, 2022, 2 Pléiades Neo images, acquired on September 18, 2022 and 6 PlanetScope images, acquired on September 18, 2022. No major rainfall events occurred in between the pre- and post-event acquisition (except for September 15 event), also considering that it is summertime in Italy (usually hot and dry) during this time span. All images were mosaicked, where necessary, and pansharpened, to obtain the highest resolution possible. In Table 1, the main features of each dataset used are reported.

Methodological approach

The approach adopted for the detection and mapping of the landslides triggered by the September 15 event is based on the i) integration of image segmentation and supervised classification methods, ii) use of NDVI (Normalized Difference Vegetation Index) change detection and iii) visual inspection and interpretation of pre- and post-event imagery. Moreover, field surveys were completed in the aftermath of the rainfall event and in the

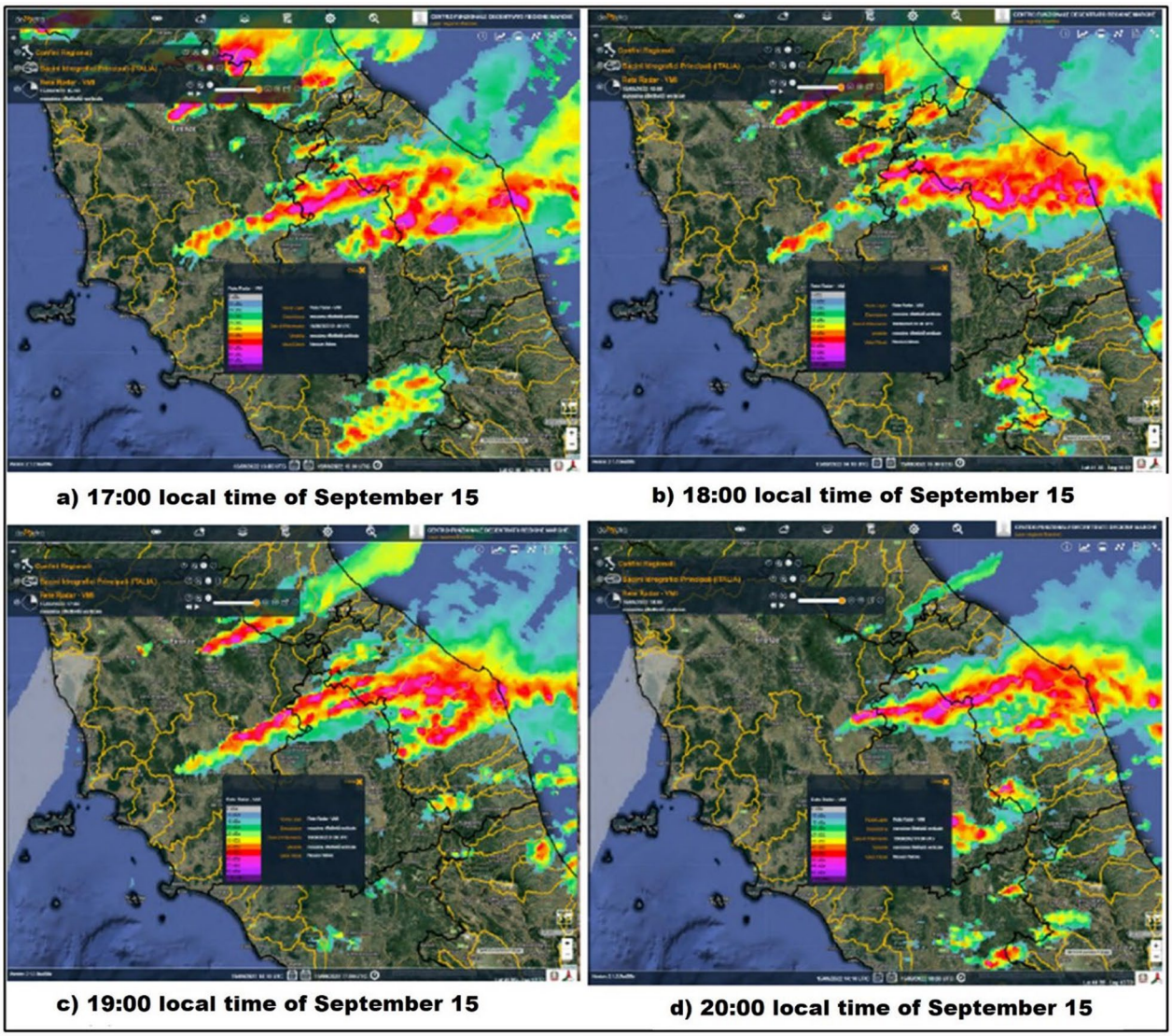

Fig. 2 Metereological radar observation of the study area during the evening of September 15: **a** 17:00 local time; **b** 18:00 local time; **c** 19:00 local time; **d** 20:00 local time. Modified from 15 September 2022 event report, by Centro Fuzionale Regionale Marche (https://www.regione.marche.it/portals/0/Protezione_Civile/Manuali%20e%20Studi/Rapporto_Evento_preliminare_20220915.pdf)

Table 1 Dataset of the optical multispectral images used

Images	Date of acquisition	Period of acquisition	Number of scenes	Resolution (pan-sharpened)
SPOT-6	30/04/2022	Pre-event	2	1.5 m
WorldView-2	22/05/2022	Pre-event	2	0.4 m
Pléiades Neo	18/09/2022	Post-event	2	0.5 m
PlanetScope	18/09/2022	Post-event	6	3 m

next months. The adopted procedure follows the operational scheme as in Fig. 3.

Image segmentation is an essential pre-requisite for classification/feature extraction and further analysis with geographic information systems (GIS) (Blaschke

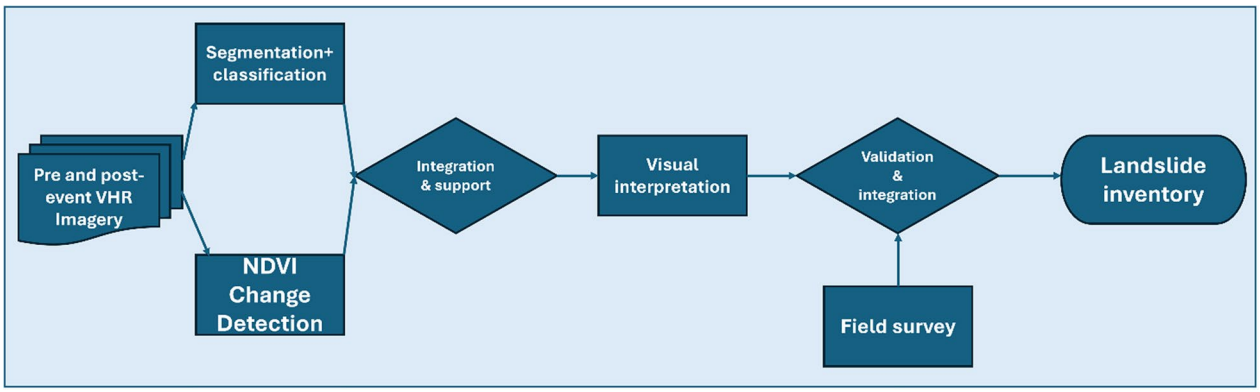

Fig. 3 Flowchart of the procedure adopted

et al. 2018; Piralilou et al. 2019). Image segmentation is the process of assigning homogeneous pixels into spectrally similar image segments, thus changing the characteristics of the image into more relevant, object-based cluster. Image segmentation is based on the Mean Shift approach (Tao et al. 2007); the technique uses a moving window that calculates the average value of pixels to determine which of them should be included in each segment. As the algorithm processes, it iteratively recalculates the value to ensure that each segment fits. The result is a clustering of image pixels into a segment characterised by an average colour. The characteristics of the segments of the image depend on three parameters: spectral detail, spatial detail and minimum segment size. It is possible to vary the amount of detail, depending on the size, geometry and spectral properties that characterise an element of interest (Comaniciu and Meer 2002; Christoudias et al. 2002).

The segmented image provided the base for an optimal classification of the scene using a supervised method, i.e., the Maximum Likelihood (Richards, 1961). Maximum likelihood classification assumes that the statistics for each class in each band are normally distributed and calculates the probability that a given pixel belongs to a specific class. Therefore, each pixel is assigned to the class that has the highest probability (that is, the maximum likelihood). Nine different features were distinguished and selected as classes to be assigned to the classification model as a input, namely: turbid water, open pit, water body, landslide, structure and infrastructure, cultivated soil, bare soil, low vegetation, high vegetation.

Regarding NDVI, vegetation indexes are often used as a detection tool for vegetated areas and can provide useful information in case of a destructive event, such as landslides, may occur (Mondini et al. 2011a, b; Gomes et al. 2020). Indeed, when a landslide occurs, the vegetation on the slope is removed or partially destroyed, leading to a decrease of NDVI value.

Landslide identification was finalized by geomorphological interpretation in a GIS environment, using the VHR pre- and post-imagery assisted by a 10 m DEM to have a 3D representation of the territory. To minimize any subjectivity in the landslide mapping stage, the boundary detection was done, checked and finalized individually by each of the members of the team, supported by the automatic detection previously described. Moreover, such analysis was also supported by the field operations in the aftermath of the event.

Indeed, after September 15 event, in situ inspections were carried out in all the 17 municipalities of the affected areas. Inspections were carried out from September 28, 2022, to October 14, 2022. The reconnaissance field survey was carried out by several teams belonging to the Centro di Protezione Civile of the University of Florence, guided by technical staff of the municipalities involved and regional authorities. The mapping of the landslide in situ was achieved through digital mapping on field GIS systems and georeferenced photo acquisition; the mapping was further refined and completed using the dataset of VHR imagery. Ad hoc localities with geomorphological evidence were selected, led by warnings and reports by local citizens damaged by the event. A total of 167 sites were investigated in detail and the main critical issues identified during the inspections were mass movements and widespread phenomena of flooding and bank erosion. Further inspections were carried out on July 31 and August 2, 2023, to assess possible evolutions of slope instability phenomena following a second hydrometeorological event of lower intensity that occurred in May 2023. On that occasion, evolutions of some landslides triggered in September 2022 were observed, such as retrogressions and enlargements,

especially in the southern sector of the basin, however, in this inventory, only September 2022 landslides are included. All the surveyed areas' outcomes were used as ground truth and to refine the remote mapping, to have the final landslide inventory. Indeed, through the field operations, the final mapping was refined in case of very small landslides and/or landslides covered by high-vegetation canopy, which would likely remain just using remote sensing images (Santangelo et al. 2023).

Results

A total of 805 landslides were recognized in the area covered by the post-event images of September 18 (including not only the Misa basin area but also some confining sectors to the West, northwest and east of the territory). As regards the Misa basin, 701 phenomena were reported. However, to have the broadest possible picture of the events, analysis will refer to the 805 phenomena reported over the entire basin and adjacent areas covered by satellite images (Figure 4). The first phase of segmentation and classification allowed to

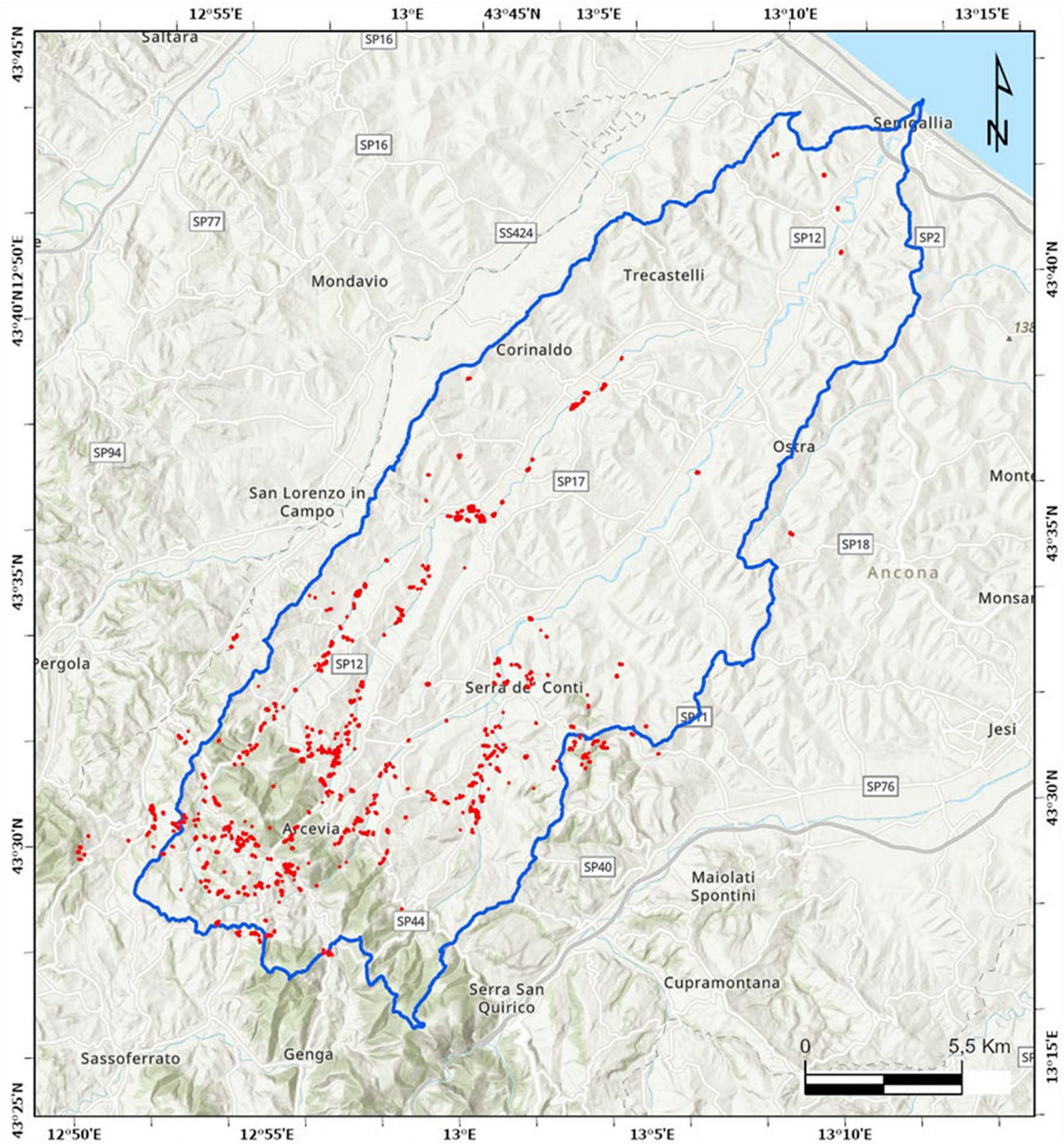

Fig. 4 Landslide inventory map of the Misa basin and the surrounding areas

generate 623,327 polygons derived from the scanning of the whole post-event image. In the following step, the segmented image was classified using the Maximum Likelihood algorithm, giving as input 9 ROIs (Region of Interests), each for the main land use classes, including landslides. Through this process, 134,000 m^2 were classified as an area affected by landslide; The NDVI change detection was implemented selecting an NDVI decrease threshold of 0.55, chosen after different iterations and aiming to select only the abrupt changes in vegetation, so that all the areas showing a NDVI decrease of 0.55 can be considered as landslide candidate. In this way, an extension of more than 14,600,000 m^2 was individuated. Both the areas automatically determined have provided a first selection of possible landslide location, supporting the landslide manual identification. All the 805 landslide phenomena detected cover an area of approximately 494,000 m^2 with an average extension of 614 m^2 (Fig. 5).

Figure 6 shows the magnitude frequency distribution of the total landslide inventory. According to the literature, landslide magnitude frequency distribution follows a power-law distribution (Catani et al. 2016). Two main features control the shape of the magnitude-frequency distribution: the cut-off point, where the distribution deviates from the power-law distribution in the interval corresponding to high frequencies, and the rollover effect, which is observed in small landslide magnitudes, resulting in the underestimation of smaller landslides since small occurrences are easily overlooked in field surveys or made invisible by vegetation regrowth, human activities and weathering processes on hillslopes (Guzzetti et al. 2002). In this case, the rollover effect occurs over an area of about 60 m^2, which is quite small and proves the quality and completeness of the landslide inventory created with VHR optical images.

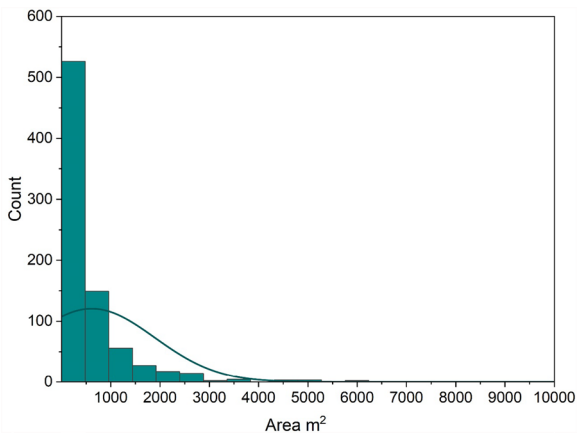

Fig. 5 Landslide distribution according to the areal extent

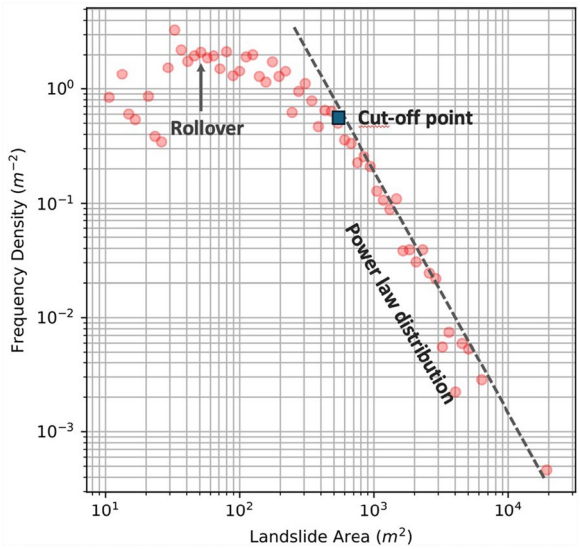

Fig. 6 Landslide inventory frequency area distribution

Landslide typology

Landslide type attribution was conducted using the most widely used classification schemes in the literature, such as Cruden & Varnes (1996), based on recognition of the type of movement. The 805 landslides inventoried were classified as follows: i. flow, where it was possible to observe a typical lobate shape or with the elongated channeled deposit; ii. slides, where the detachment area is evident; iii. shallow, where a typical shape is not evident but a substantial dynamic in the first portions of the ground is clear; iv. ND (undetermined), since it was not possible to distinguish the type of movement; and v. bank landslides, i.e. landslide phenomena linked to the effects of floods on the riverbank of the Misa and Nevola rivers. In the 805 recognized phenomena, the types that stand out with the highest number of polygons are shallow landslides (519) and slides (132), which alone represent about 80% of the sample; bank landslides represent almost 10% of the landslides inventoried (Fig. 7). In Fig. 8, some examples of the different types of landslide recognized are reported.

The roundness of the landslide polygons has been also assessed, through the Polsby-Popper (PP) test (Polsby and Popper 1991, and used for geomorphological studies in other studies, such as Lioupa et al. 2024 and Rodenhizer et al. 2024) (Fig. 9). The PP score is determined by using the polygon area and perimeter, through the following formula:

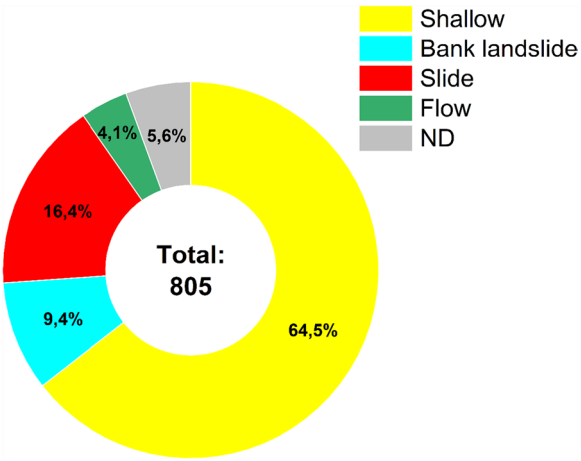

Fig. 7 Distribution of the landslide typology

$$R = 4\pi A/P^2$$

where R is the roundness of the polygon, A is the area and P is the perimeter. The values of the equation range from 0 to 1, where 0 means a very irregular shape, 0.5 corresponds to elongated polygons and 1 to perfect circular shapes, being the shape with the highest compactness.

The analysis of the roundness has been conducted over the whole landslide database, considering the various typologies identified. Shallow and flow landslides are characterized by average values of 0.46 and 0.53, respectively, while slides and bank landslides by 0.57 and 0.56, respectively. ND are also characterized by an average value of roundness of 0.54. From the boxplot analysis of Fig. 9, however, a larger distribution of values can be seen in slides and bank landslide categories, showing a higher standard deviation.

Landslide distribution

To provide a representative framework of landslide instability in the study area, the landslide density was evaluated. To this aim, a 250 m square cell landslide density map was produced (Fig. 10). Since landslides are very small, this method is a cartographic expedient to provide a synoptic representation of landslide occurrence. This cartographic expedient allows for a clearer spatial analysis and visualization of landslide density. The Arcevia area, located in the southern part of the catchment, is distinguished by a significant number of high-density cells, with as many as 13 landslides in a single cell. In total, there are 33 cells with more than 5 landslides in the municipality of Arcevia, while in the municipalities of Serra de' Conti and Barbara there are 2 each. Finally, in the municipality of Corinaldo, in the northwest sector, there is a cell containing 10 landslides, all related to the river Nevola's bank dynamics (Fig. 10).

Landslides and geomorphological and anthropogenic factors

With the aim of assessing the scenario of landslide events occurring following the rainfall of September 15, 2022 in the area, landslide polygons were cross-referenced with some of the most important thematic and morphometric maps. Cross-references were made between the newly formed landslides and i) the slope angle map; ii) the geological formations outcropping in the study area; iii) the

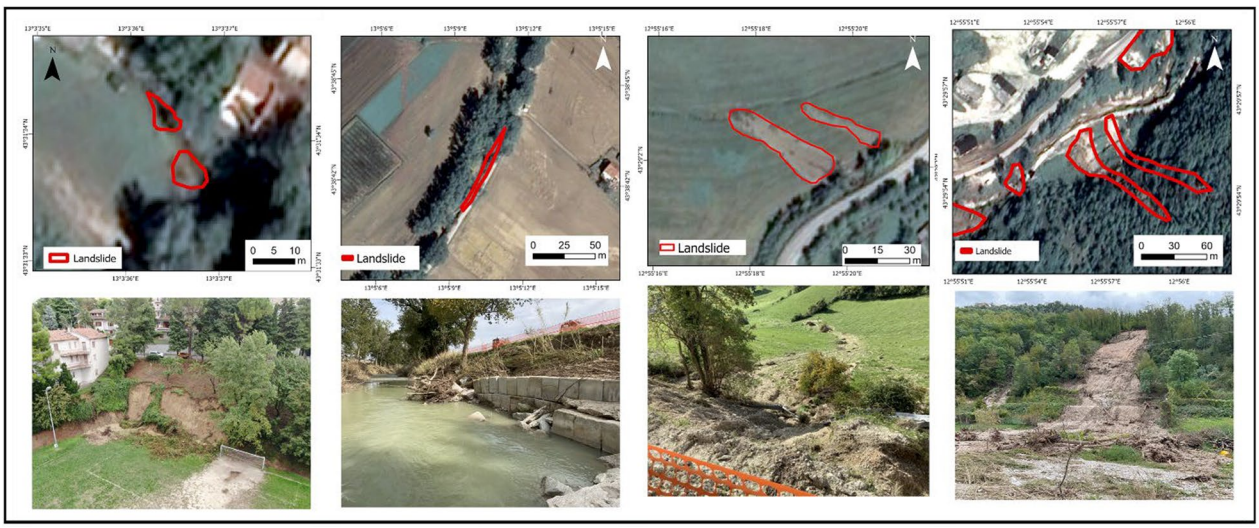

Fig. 8 Example of landslide classified according to the typology. On the top, satellite view on the bottom, picture taken in the field. From left to right: shallow, bank landslide, flow, slide

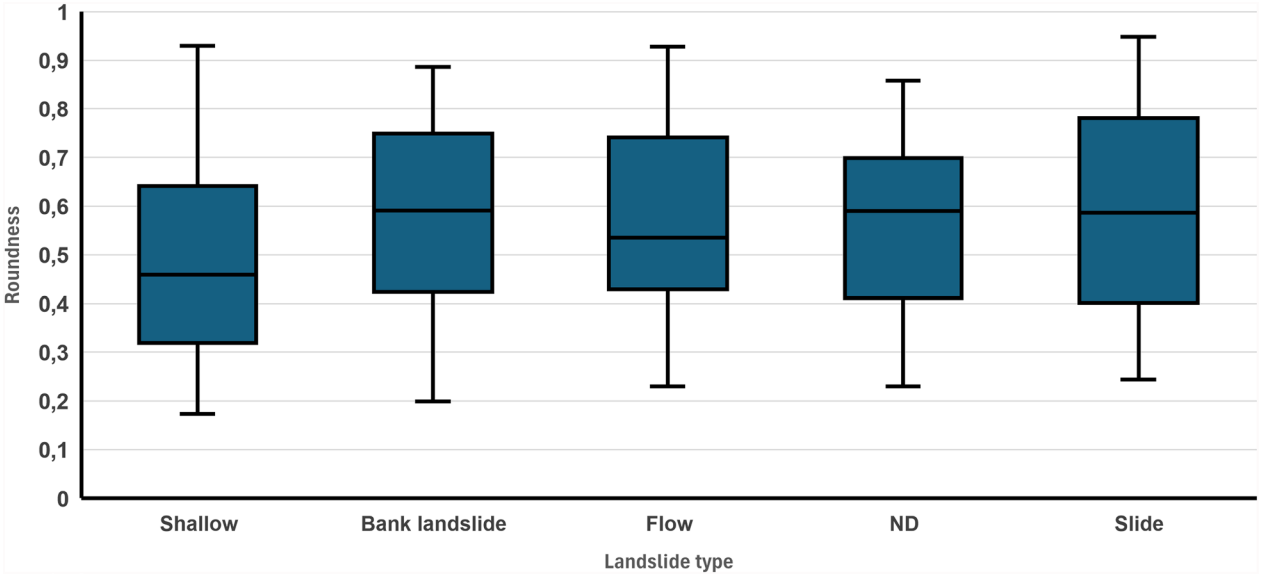

Fig. 9 Roundness index distribution of landslides classified according to the type

land cover, obtained from the Corine Land Cover (CLC 2018); iv) the official landslide national database IFFI; v) the event rainfall map. In the first investigation, the mean, minimum and maximum value of slope angle was computed for each landslide. The slope map was generated starting from a 10 m-resolution DEM, developed in the framework of the TIN-Italy project (Tarquini and Nannipieri, 2017). The distribution of the slope angle values is shown in Fig. 11. The highest frequency of mean slope values of the landslide inventory can be seen in the class 5°−10°, as well as the maximum values. The average values of mean, minimum and maximum slope registered are 11.3°, 9.3° and 13.5°, respectively.

In the second overlap comparison, the geological database compiled by the Marche region was used (CARG Project, 2024, at a scale of 1:50.000). In the case of the study area, 75% of the landslides were set on Quaternary deposits Scaglia formation, made up of limestone rocks, for 6.1% of the cases, on the Schlier (5%), corresponding to calcareous marl rocks, and on the arenaceous-conglomeratic lithofacies (3.9%) (Fig. 12a). The remnant 10% of landslides are distributed among other lithologies, however with no significant statistical prevalence. The impact of landslides over the type of land cover of Misa basin has been assessed, using 100 m resolution CLC (Fig. 12b). The results show that 90.8% of landslides occurred in agricultural areas (class 2), mostly in class 2.1.1 (non-irrigated arable land), for a total of 379 polygons, followed by classes 2.4.2 and 2.4.3 (complex cultivation patterns and land occupied by agriculture with significant areas of natural vegetation), with 175 and 173 polygons, respectively. Only 9.2% of inventoried landslides was overlapping other CLC categories, belonging to classes 1 and 3 (artificial surfaces and forest areas, respectively).

To analyze the distribution of landslides triggered by the event and those previously mapped in the area, the event landslide inventory map was compared with the Italian national landslide inventory (IFFI, *Inventario dei Fenomeni Franosi in Italia*, in Italian; Trigila et al. 2007) redacted by ISPRA (*Istituto Superiore per la Protezione e Ricerca Ambientale*, Superior Institute for Environmental Protection and Research in Italian), available on the Idrogeo portal (https://idrogeo.isprambiente.it/app/). The Marche region inventory's last update was provided in 2007, as indicated by ISPRA (https://www.progettoiffi.isprambiente.it/?page_id=63). 17.6% of the 805 landslides mapped as part of this project were found to be intersecting with IFFI landslides, while the remainder were formed in areas not previously mapped (Fig. 13). Among the event landslides overlapping with IFFI landslides, 59.9% are in the municipality of Arcevia, while 15.5% and 12% are in the municipalities of Serra de' Conti and Sassoferrato, respectively. These percentages are extremely lower in the remaining municipalities, below 6%. In general, smaller landslides are within larger IFFI polygons: indeed, the average size of these is about 450 m^2.

Finally, the landslide map was overlaid with the 15 September event rainfall distribution of which was determined by interpolating the daily precipitation of 18 rain gauges in the study area and its surroundings (Fig. 14). The precipitation map shows higher daily precipitation

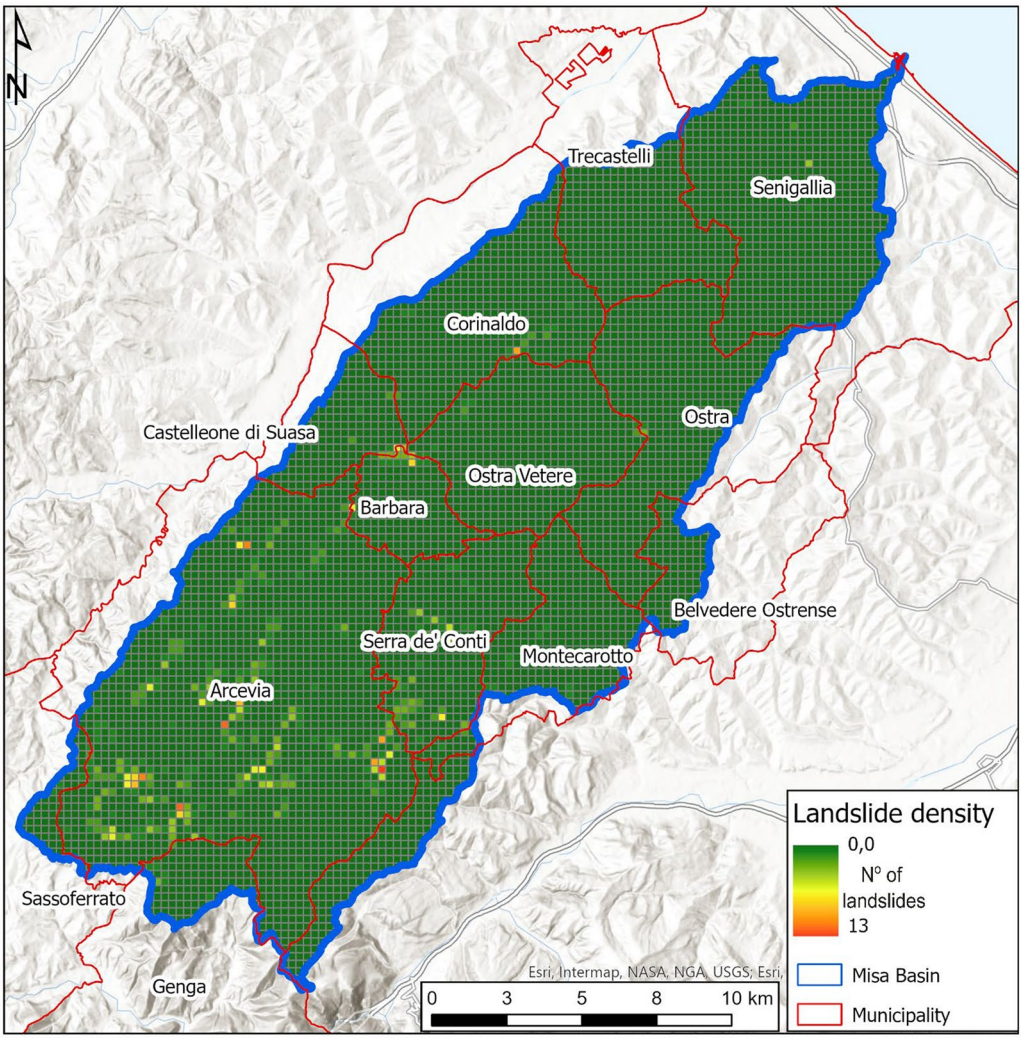

Fig. 10 Landslide density map. Only municipalities where at least one cell with landslide density value different from zero are reported. The basemap consists of the world hillshade map available on ArcGIS map service

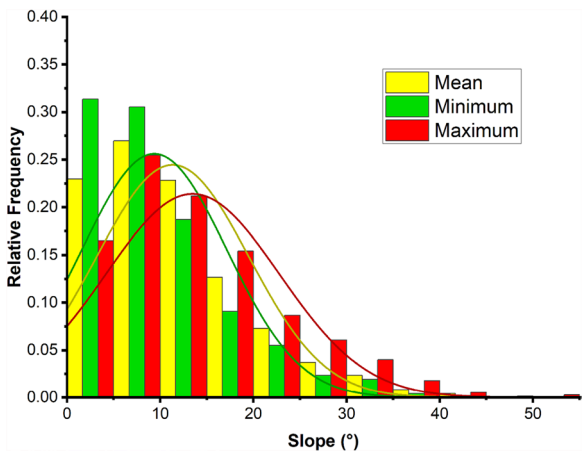

Fig. 11 Frequency distribution of mean, minimum and maximum slope angle value for each landslide. The three curves show the frequency distribution of slope angle values

amounts in the southern sector of the Misa basin (in the Serra de' Conti-Montecarotto area), which reached about 200 mm. The coastal area, on the other hand, shows much lower values, confirming that the perturbation ran from west to east and exhausted itself when it reached the coastline. The distribution of landslides partly reflects the rainfall distribution: 70% of landslides occurred in areas where rainfall values were between 100 and 140 mm. Very few landslides were recorded in areas with low rainfall (about 10% of landslides below 100 mm rainfall), while about 20% occurred in areas with more than 140 mm.

Landslides and urban areas

To assess the impact of newly formed landslides on the built environment in the study area, cross-comparisons were made between the landslide polygons and the

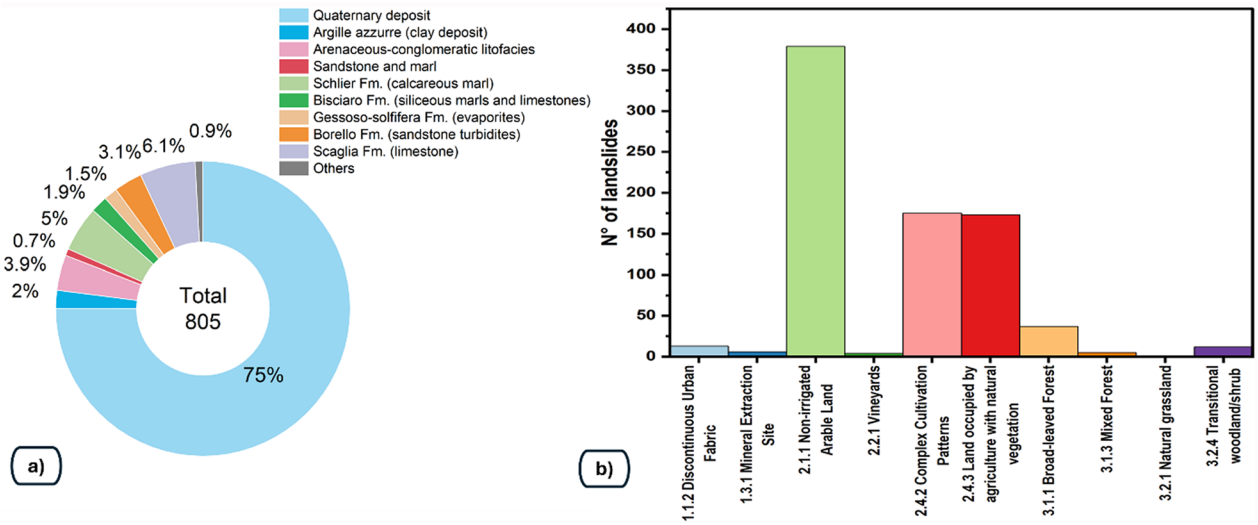

Fig. 12 **a** Distribution of landslides according to the geological setting; **b** Distribution of landslides according to the Corine Land Cover class

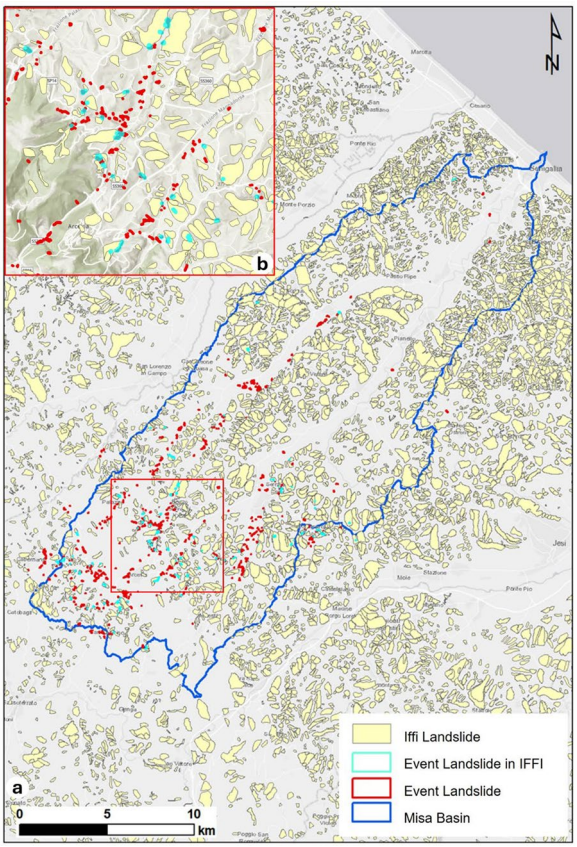

Fig. 13 **a** Map of the September 15, 2022, landslides intersecting IFFI landslides. **b** Inset showing this correlation in a specific area, encompassed in the red polygon of Fig. 13.

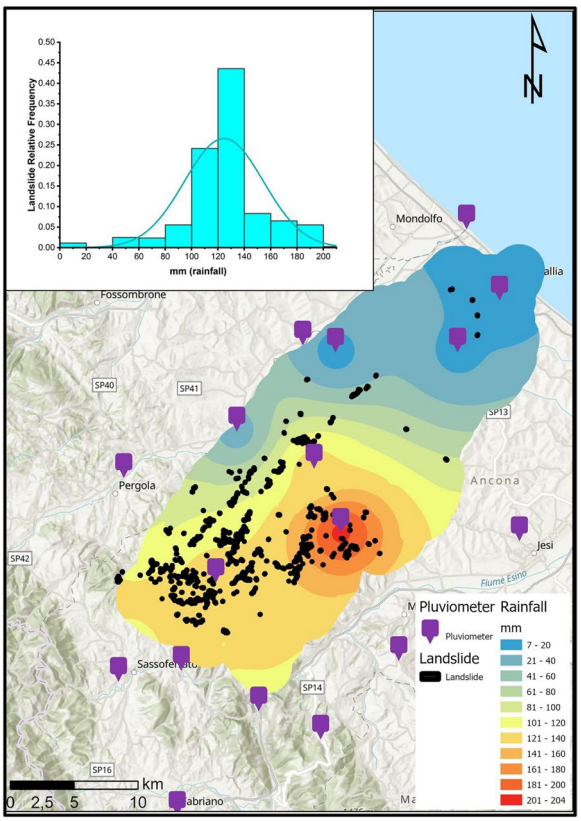

Fig. 14 Map of the event landslides intersecting interpolated September 15, 2022, daily rainfall map. On top left, distribution of landslides according to daily rainfall amount. The curve shows the distribution of rainfall values in the study area

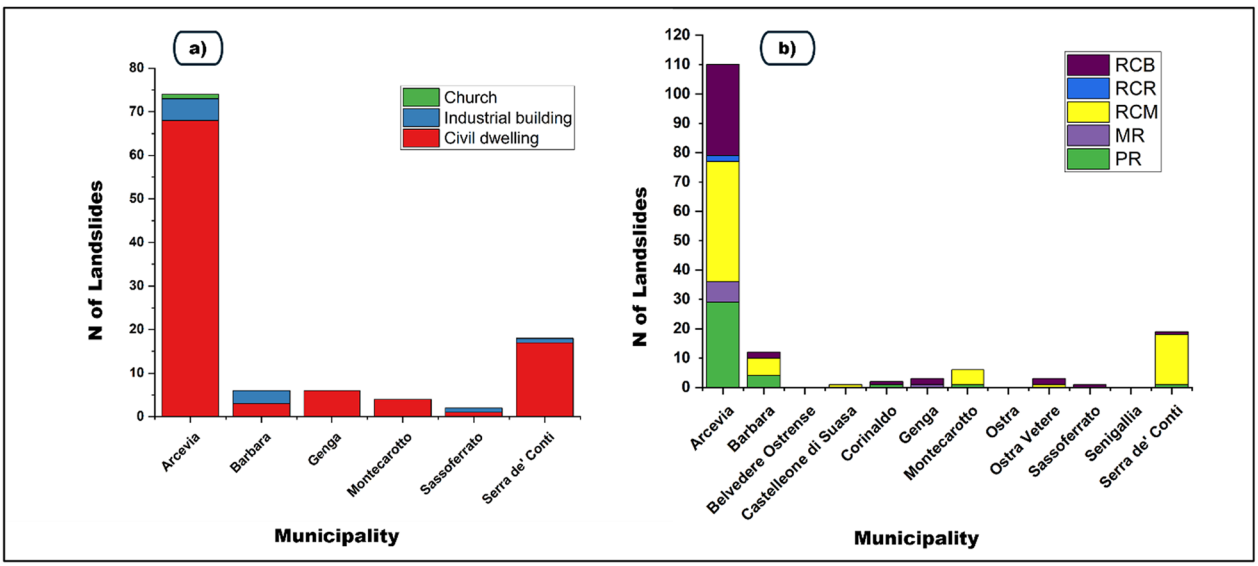

Fig. 15 Landslide interaction with the urban environment: **a** number of buildings affected by landslides; **b** roads affected by landslides distribution for each municipality. RCB = Road Connecting to Buildings; RCR = Road Connecting to main Roads; RCM = Road Connecting to Minor network;F MR = Municipal Road; PR = Provincial Road

structures and infrastructure (Fig. 15). Such information was derived from the Marche regional database and the Technical Regional Cartography, at the scale of 1:10′000. A 20 m buffer, selected considering the average road size and the area of influence of the landslides, considering their average size, was applied to the landslides to better analyse the influence of these phenomena on buildings. Among the most evident results, in the municipality of Arcevia a total of 74 buildings were affected by landslides, mostly civil dwellings (68). In the municipality of Serra de' Conti as well, almost exclusively civil dwellings were involved (17 out of 18). Nevertheless, industrial buildings and churches were also impacted by the landslides, for a total of 10 and 1, respectively. A similar analysis was conducted on the road network by applying a buffer of 20 m to the road network. This analysis showed that landslides mostly impacted roads in the municipality of Arcevia (110 in total), followed by Serra de' Conti (19) and Barbara (12). In total, there were 157 roads affected by landslides, of which 71 were classified as roads connecting to the main road network, 40 as roads connecting to scattered buildings and mountain peaks, and 36 as provincial roads.

Discussion

The composite procedure, based on the joint application and exploitation of the spectral properties and the high-resolutionof satellite images, has allowed the detection and identification of 805 landslides, all triggered by the extreme rainfall event of September 15, 2022. The exceptional nature of the event was reconstructed by the Regional Functional Center of Marche, which estimated Return Time of every rainfall record (3,6,12 and 24 h) higher than 1000 years (https://www.regione.marche.it/portals/0/Protezione_Civile/Manuali%20e%20Studi/Rapporto_Evento_preliminare_20220915.pdf). To make the exceptional nature of the hydropluviometric event that occurred even more evident, in the Cantiano area, on the evening of 15 September alone, 30% of the rainfall that usually falls in a year (1300 mm) fell. To characterize ground effects of the event on the territory, an inventory of landslides through the primary use of very high-resolution optical images acquired in the immediate post-event scenario, with the aid of field surveys, was redacted. In situ operations were conducted 2 weeks after the main event, in all the municipalities involved, aiming at the preliminary mapping of the still ongoing geomorphological hazards. Such work has represented a solid base to i) refine the mapping of landslides using remote sensing imagery; ii) support the classification of the landslides typology; iii) reduce the number of false positives, i.e., landforms apparently associated to gravitational phenomena but mostly related to abrupt land cover changes; iv) map landslides in shadowed areas and/or not visible through imagery. Regarding the latter, 24 landslides observed only in the field are reported in the final inventory. Despite field operation, false positives still may be present in the inventory, due to spectral and visual characteristics of features similar to landslide areas (Mondini et al. 2011b). The territories most affected are located

in the southern portion of the basin, particularly in the municipalities of Arcevia, Serra de' Conti, Sassoferrato and Montecarotto, where 90% of the landslides detected are localized. This is mainly linked to the dynamics of the rainfall that occurred, as shown in Fig. 14, whose higher intensity values occurred in this portion of the territory, but also to the generally steeper morphology in these areas, as visible in Fig. 11, even though the mean slope angle is of 11.5°, not a very high gradient. The higher spreading of landslides in the southern area of Misa basin is also confirmed by the work of Santangelo et al. 2023 and Donnini et al. 2023, who identified 1687 landslides in the area south of Misa basin, in the epicenter of the rainfall peak of September 15 event. The inventory reported here, however, can be only partially compared to the abovementioned works, since the study area is different (they mostly worked on adjacent basins, Metauro, Cesano and Esino) and the mapping activity was essentially conducted in the field, without remote sensing interpretation. Despite such discrepancies, some analogies can be found between our work and that of Donnini et al. (2023): the landforms identified are mostly classifiable as shallow landslides, with prevailing slide kinematics, with a major distribution density in the area of higher rainfall intensity. The average size of the landslides detected is general small (smaller than 10^3 m^2), as well as in our case the cut-off point of the distribution of landslides (in Fig. 6), corresponding to the higher frequency of the distribution, is set at 60 m^2. Furthermore, also in their work, the role of land cover was analyzed, identifying most of the slide phenomena over agricultural areas.

To emphasize the strong relationship between the triggering of surface landslides and the lithological context, a comparison was made between landslides and the geolithological map of the study area. This showed that three-quarters of the landslides were triggered on Quaternary overburden soils: therefore, the event landslides consist of reactivations of landslide, eluvial, colluvial and alluvial deposits formed over the last few hundred thousand years, which have not yet been fully compacted. Moreover, also a connection between agricultural soils and landslides was found (Fig. 12).

The association between morphometric parameters and territorial attributes with newly inventoried landslide, although is a common practice, is a fundamental step for analyzing the study area characteristics, also in view of the prediction of future occurrence of similar scenarios, i.e., landslide susceptibility evaluation. Indeed, despite the great progress in terms of technologies and methodologies for landslide susceptibility assessment, especially since the introduction of Machine and Deep Learning models, still the selection of input environmental variable is human-driven, mostly led by the knowledge of the territory and the expected phenomena in case of similar meteoric events or otherwise extreme in character. In the case of the Misa basin, Caleca et al. (2024), adopted ten environmental variables (among which slope angle, land cover and lithology) to assess the probability of occurrence of landslides under different rainfall scenarios, including the September 15 event. In this work, the influence of rainfall dynamics was determined to be dominant on landslide trigger.

In order to also assess the existing cartography regarding hydrogeomorphological instability, the polygons of the newly formed landslides were compared with the IFFI ones: in this case, this overlap showed that only 18% intersected with the pre-existing inventory, thus highlighting the need to update the inventories of landslide phenomena following exceptional rainfall events. This is pretty obvious considering that IFFI database contains different landslide typologies, and this area never experienced such an extreme event, thus not having such kind of phenomena. Moreover, the technologies implemented in this research were not available at the time of IFFI mapping, therefore here it was possible to map also very small landslides. This underlines a need to update the cognitive framework and tools to act on land planning and management, facing the current climate change scenario which foster the activation of different landslides. Finally, it was also observed how the analysed slope instabilities had a significant impact on the territory and the urban environment of the study area. Given the results of this work, the role of accurate and updated risk mapping becomes increasingly important to better estimate the expected damage to buildings and roads in such scenarios.

Concerning the methodologies implemented for the redaction of the inventory, the automatic mapping stage was useful for defining a first screening of the landslide-affected areas, through the detection of soil cover change. However, precise mapping was not possible due to intrinsic limitations of semi-automatic mapping, especially when dealing with small polygons, and to the seasonal changes in land cover. The segmentation stage was implemented to aggregate pixels with the same spectral properties, while the supervised classification algorithm was used to assign a land cover type to each polygon. In this way, ca 13.7 km^2 of land were classified as landslides; however, only 1% (0.13 km^2) of these were correctly assigned within the 805 landslide polygons recognized by photointerpretation. The numbers of true positives decrease even more when implementing the NDVI change detection, which overestimates the extent of the area potentially affected by landslides. These outcomes can be considered predictable, due to several factors: i) the presence of cultivated and agricultural areas

(mainly vineyards, sunflowers, corn and fruit trees), which significantly change in the two time periods (April and September 2022), due to differences in the climate and the related agricultural practices (in spring there is a consistent flourishing of cultivated fields, while in summer all the fields are harvested). Indeed, in many cases, areas classified as landslides were bare soil areas; ii) the small size of the landslides, which are large 614 m^2 in average, making the detection, even using VHR imagery, very challenging. In this sense, further improvements may be achieved by using accordingly VHR multispectral imagery and very detailed topographic factors derived from LiDAR data, to be implemented in automatic methods, such as in Gherbanzadeh et al. (2019), by implementing deep learning methods such as Convolution Neural Networks (CNNs), or U-net which are improving the performances in terms of rapid precise mapping (Liu et al. 2021, Bhuyan et al. 2023).

Conclusion

The exceptional hydro-meteorological events of 15 September 2022 in the Misa basin (Ancona province, Central Eastern Italy) caused numerous landslide phenomena on the slopes, resulting in the isolation of some localities, the evacuation of families from their homes, and serious damage to road infrastructures, farms, public and private buildings, hydraulic defense works and the network of essential services.

This paper summarises the work conducted in the aftermath of such event, focusing on the inventory of the landslide phenomena that occurred following the abundant and exceptional rain poured into the area in a few hours. For this purpose, techniques based on the elaboration and interpretation of Very High-Resolution satellite images and field surveys were implemented. A total of 805 landslides were identified, covering a total area of approximately 494,000 m^2. The landslides identified were mainly shallow landslides, mainly set on quaternary soils (essentially overburden deposits). Among the most affected municipalities are those essentially located in the southern mountain sector of the basin, i.e. Arcevia, Montecarotto, Serra de' Conti and Sassoferrato, where the rainfall quantities registered were higher (70% of landslides occurred in areas where rainfall values were between 100 and 140 mm). Finally, it has been observed that the landslides had a big impact on the territory, and on the cultivated areas, since the economy of the area is mostly concentrated on agriculture, accounting for ca. 90% of the landslides and on urban sectors, affecting buildings (where 110 landslides hit a building) and roads (hit by 314 landslides). Given the exceptional nature of meteorological phenomena, which have proven to be extraordinary events both in terms of their intensity (return period of more than 1,000 years) and their enormous territorial extent, it is necessary to provide useful products for planning and land management that are as up-to-date as possible, both in terms of input data and the methods used. This is even more significant considering that, according to recent climate trends, such events will be repeated with increasing frequency. Such timely inventories can be a fundamental step towards also producing new vulnerability/hazard and risk maps that can be used for spatial planning.

Acknowledgements

The publication was made by a researcher with a research contract co-funded by the European Union—PON Research and Innovation 2014–2020 in accordance with Article 24, paragraph 3a), of Law No. 240 of December 30, 2010, as amended and Ministerial Decree No. 1062 of August 10, 2021. The authors kindly acknowledge Alessia Schiaroli and Pierpaolo Tiberi (Regione Marche – Direzione Protezione Civile e Sicurezza del Territorio) for providing and sharing useful information.

Author contributions

Conceptualization, P.C.; methodology, P.C., R.F., L.S.; investigation, P.C., R.F., F.R., S.M., L.S., V.T.,; writing—original draft preparation, P.C.; writing—review and editing, P.C., R.F., S.M., F.R., V.T.; supervision, Sa.M. and N.C. All authors have read and agreed to the published version of the manuscript.

Availability of data and materials

No datasets were generated or analysed during the current study.

Declarations

Competing interests

The authors declare no competing interests.

Received: 13 November 2024 Accepted: 30 May 2025
Published online: 08 July 2025

References

Bonì, R, Massimiliano B, Alessio C, Luca L, and Claudia M (2024) Landslide state of activity maps by combining multi-temporal A-DInSAR (LAMBDA) - ScienceDirect. https://www.sciencedirect.com/science/article/pii/S003442571830378X?casa_token=z0hczv_xZuYAAAAA:QCc6S2WUJG-SgLYHp4bP5ky7Y9AvL-O5cyexd1FdWJghRWWsqchwonYibQdl6n-eHeVR03wK1g. Accessed October 2.

Brocchini M, Calantoni J, Postacchini M, Sheremet A, Staples T, Smith J, Reed AH et al (2017) Comparison between the wintertime and summertime dynamics of the Misa River estuary. Mar Geol 385:27–40. https://doi.org/10.1016/j.margeo.2016.12.005

Caleca F, Confuorto P, Raspini F, Segoni S, Tofani V, Casagli N, Moretti S (2024) Shifting from traditional landslide occurrence modeling to scenario estimation with a "glass-box" machine learning. Sci Total Environ 950:175277. https://doi.org/10.1016/j.scitotenv.2024.175277

Gino C, Centamore E, Chiocchini U, Colalongo ML, Aurora M, Nanni T, Maria P, Ricci Lucchi F, Cristallini C, and Di Lorito L (1986) Il Plio-Pleistocene delle Marche. Centro Stampa dell'Università di Camerino, fino al 1999

CARG Project - Geologic and Geothematic Cartography Available online: https://www.isprambiente.gov.it/en/projects/soil-and-territory/carg-project-geologic-and-geothematic-cartography-1 (accessed on 4 May 2024).

Catani F (2021) Landslide detection by deep learning of non-nadiral and crowdsourced optical images. Landslides 18:1025–1044. https://doi.org/10.1007/s10346-020-01513-4

Catani F, Tofani V, Lagomarsino D (2016) Spatial patterns of landslide dimension: a tool for magnitude mapping. Geomorphology 273(2016):361–373
Centamore E, Dramis F, Bernardino G, and Pambianchi T, Nanni G (1991) Carta geoambientale del bacino del Tenna (Marche centro-meridionali). Fabriano
Christoudias CM, Georgescu B, Meer P (2002) Synergism in low level vision. In: 2002 International conference on pattern recognition, vol 4. IEEE, pp 150–155
CLC (2018) https://land.copernicus.eu/en/products/corine-land-cover/clc2018
Comaniciu D, Meer P (2002) Mean shift: A robust approach toward feature space analysis. IEEE Trans Pattern Anal Machine Intell 24(5):603–619
Confuorto P, Casagli N, Casu F, De Luca C, Del Soldato M, Festa D, Lanari R, Manzo M, Onorato G, Raspini F (2023) Sentinel-1 P-SBAS data for the update of the state of activity of national landslide inventory maps. Landslides 20:1083–1097. https://doi.org/10.1007/s10346-022-02024-0
Cruden DM, Varnes DJ (1996) Landslide types and processes, transportation research board, U.S. National Academy of Sciences, Special Report, 247:36–75
Del Soldato M, Riquelme A, Bianchini S, Tomàs R, Di Martire D, De Vita P, Moretti S, Calcaterra D (2018) Multisource data integration to investigate one century of evolution for the Agnone landslide (Molise, southern Italy). Landslides 15:2113–2128. https://doi.org/10.1007/s10346-018-1015-z
Diakakis M, Mavroulis S, Filis C, Lozios S, Vassilakis E, Naoum G, Soukis K et al (2023) Impacts of medicanes on geomorphology and infrastructure in the eastern mediterranean, the case of medicane ianos and the ionian islands in western greece. Water 15:1026. https://doi.org/10.3390/w15061026
Dietrich A, Krautblatter M (2017) Evidence for enhanced debris-flow activity in the Northern Calcareous Alps since the 1980s (Plansee, Austria). Geomorphology 287:144–158. https://doi.org/10.1016/j.geomorph.2016.01.013
Donnini M, Santangelo M, Gariano SL, Bucci F, Peruccacci S, Alvioli M, Althuwaynee O et al (2023) Landslides triggered by an extraordinary rainfall event in Central Italy on September 15, 2022. Landslides 20:2199–2211. https://doi.org/10.1007/s10346-023-02109-4
Ferrario, Maria Francesca, and Franz Livio (2024) Rapid mapping of landslides induced by heavy rainfall in the Emilia-Romagna (Italy) Region in May 2023. https://www.mdpi.com/2072-4292/16/1/122. Accessed Oct 2
Gariano SL, Petrucci O, Rianna G, Santini M, Guzzetti F (2018) Impacts of past and future land changes on landslides in southern Italy. Reg Environ Change 18:437–449. https://doi.org/10.1007/s10113-017-1210-9
Gomes PI, Aththanayake U, Deng W, Li A, Zhao W, Jayathilaka T (2020) Ecological fragmentation two years after a major landslide: correlations between vegetation indices and geo-environmental factors. Ecol Eng 153:105914
Guerrera F, Wezel FC (1979) Eventi neotettonici quaternari nell'area nord-marchigiana. Memorie della Societa'geologica Italiana 19:589–595
Guzzetti F, Malamud BD, Turcotte DL, Reichenbach P (2002) Power-law correlations of landslide areas in central Italy. Earth Planet Sci Lett 195:169–183
Guzzetti F, Mondini AC, Cardinali M, Fiorucci F, Santangelo M, Chang K-T (2012) Landslide inventory maps: new tools for an old problem. Earth Sci Rev 112:42–66. https://doi.org/10.1016/j.earscirev.2012.02.001
Hölbling D, Eisank C, Albrecht F, Vecchiotti F, Friedl B, Weinke E, Kociu A (2017) Comparing manual and semi-automated landslide mapping based on optical satellite images from different sensors. Geosciences 7:37. https://doi.org/10.3390/geosciences7020037
Hürlimann M, Guo Z, Puig-Polo C, Medina V (2022) Impacts of future climate and land cover changes on landslide susceptibility: regional scale modelling in the Val d'Aran region (Pyrenees, Spain). Landslides 19:99–118. https://doi.org/10.1007/s10346-021-01775-6
Ilari M (2020) Hydrodynamic modeling of the final reach of the Misa River (Senigallia, Italy): the role of sea action and bed forms. Unpublished master's thesis. Marche Polytechnic University
Kushabaha A, Giovanni S, Gaetano S, Mario MM, Emmanouil F, Pietro M, Antonella M, De Vincenzo S, Alfio MB, Giovanni S (2024) ARCHIMEDE—an innovative web-GIS platform for the study of medicanes. Remote Sens 16:2552. https://doi.org/10.3390/rs16142552
Lazzari M, Gioia D, Anzidei B (2018) Landslide inventory of the Basilicata region (Southern Italy). J Maps 14:348–356. https://doi.org/10.1080/17445647.2018.1475309
Lioupa V, Karsiotis P, Arosio R, Hasiotis T, Wheeler AJ (2024) A comparative crash-test of manual and semi-automated methods for detecting complex submarine morphologies. Remote Sens 16:4093. https://doi.org/10.3390/rs16214093
Meena SR, Soares LP, Grohmann CH, van Westen C, Bhuyan K, Singh RP, Floris M, Catani F (2022) Landslide detection in the Himalayas using machine learning algorithms and U-Net. Landslides 19:1209–1229. https://doi.org/10.1007/s10346-022-01861-3
Micarelli, A, Potetti M, Chiocchimi M (1977) Richerche microbiostratigrafiche sulla maiolica della regione umbro-marchigiana. *Richerche microbiostratigrafiche sulla maiolica della regione umbro-marchigiana*.
Mondini AC, Chang K-T, Yin H-Y (2011a) Combining multiple change detection indices for mapping landslides triggered by typhoons. Geomorphology 134:440–451. https://doi.org/10.1016/j.geomorph.2011.07.021
Mondini AC, Guzzetti F, Reichenbach P, Rossi M, Cardinali M, Ardizzone F (2011b) Semi-automatic recognition and mapping of rainfall induced shallow landslides using optical satellite images. Remote Sens Environ 115:1743–1757. https://doi.org/10.1016/j.rse.2011.03.006
Mondini AC, Santangelo M, Rocchetti M, Rossetto E, Manconi A, Monserrat O (2019) Sentinel-1 SAR amplitude imagery for rapid landslide detection. Remote Sens 11:760. https://doi.org/10.3390/rs11070760
Morelli S, Bonì R, Guidi E, De Donatis M, Pappafico G, Francioni M (2023) L'alluvione delle Marche del 15 settembre 2022, cause e conseguenze. Cult Territ Linguaggi 24:136–147
Novellino A, Pennington C, Leeming K, Taylor S, Alvarez IG, McAllister E, Arnhardt C, Winson A (2024) Mapping landslides from space: a review. Landslides 21:1041–1052. https://doi.org/10.1007/s10346-024-02215-x
Pawluszek K (2019) Landslide features identification and morphology investigation using high-resolution DEM derivatives. Nat Hazards 96:311–330. https://doi.org/10.1007/s11069-018-3543-1
Pellicani R, Spilotro G (2015) Evaluating the quality of landslide inventory maps: comparison between archive and surveyed inventories for the Daunia region (Apulia, Southern Italy). Bull Eng Geol Env 74:357–367. https://doi.org/10.1007/s10064-014-0639-z
Peruccacci S, Stefano LG, Massimo M, Monica S, Fausto G, Maria TB (2023) The ITAlian rainfall-induced LandsIIdes CAtalogue, an extensive and accurate spatio-temporal catalogue of rainfall-induced landslides in Italy. Earth Syst Sci Data 15:2863–2877. https://doi.org/10.5194/essd-15-2863-2023
Plank S, Twele A, Martinis S (2016) Landslide mapping in vegetated areas using change detection based on optical and polarimetric SAR data. Remote Sens 8:307. https://doi.org/10.3390/rs8040307
Polsby DD, Popper R (1991) The third criterion: compactness as a procedural safeguard against partisan gerrymandering. SSRN Electron J. https://doi.org/10.2139/ssrn.2936284
Ramos-Scharrón CE, Arima EY, Stephen Hughes K (2020) An assessment of the spatial distribution of shallow landslides induced by Hurricane María in Puerto Rico. Phys Geogr 43(2):163–191. https://doi.org/10.1080/02723646.2020.1801121
Richards FS (1961) A method of maximum-likelihood estimation. J R Stat Soc Ser B: Stat Methodol 23(2):469–475
Rodenhizer H, Yang Y, Fiske G, Potter S, Windholz T, Mullen A, Watts JD, Rogers BM (2024) A comparison of satellite imagery sources for automated detection of retrogressive thaw slumps. Remote Sens 16:2361. https://doi.org/10.3390/rs16132361
Santangelo M, Althuwaynee O, Alvioli M, Ardizzone F, Bianchi C, Bornaetxea T, Brunetti MT et al (2023) Inventory of landslides triggered by an extreme rainfall event in Marche-Umbria, Italy, on 15 September 2022. *Scientific Data* 10. Nature Publishing Group: 427: 2336. https://doi.org/10.1038/s41597-023-02336-3.
Scardino G, Miglietta MM, Kushabaha A, Casella E, Rovere A, Besio G, Borzì AM et al (2024) Fingerprinting mediterranean hurricanes using pre-event thermal drops in seawater temperature. Sci Rep 14:8014. https://doi.org/10.1038/s41598-024-58335-w
Smith HG, Spiekermann R, Betts H, Neverman AJ (2021a) Comparing methods of landslide data acquisition and susceptibility modelling: examples from New Zealand. Geomorphology 381:107660
Smith HG, Spiekermann R, Betts H, Neverman AJ (2021b) Comparing methods of landslide data acquisition and susceptibility modelling: examples from New Zealand. Geomorphology 381:107660. https://doi.org/10.1016/j.geomorph.2021.107660
Su Z, Chow JK, Tan PS, Jimmy Wu, Ho YK, Wang Y-H (2021) Deep convolutional neural network–based pixel-wise landslide inventory mapping. Landslides 18:1421–1443. https://doi.org/10.1007/s10346-020-01557-6

Tao W, Jin H, Zhang Y (2007) Color image segmentation based on mean shift and normalized cuts. IEEE Trans Syst Man Cyberni Part B (Cybern.) 37(5):1382–1389

Tarquini S, Nannipieri L (2017) The 10 m-resolution TINITALY DEM as a trans-disciplinary basis for the analysis of the Italian territory: current trends and new perspectives. Geomorphology 281:108–115. https://doi.org/10.1016/j.geomorph.2016.12.022

Trigila, A., Iadanza C., and Luca G. The IFFI Project (Italian Landslide Inventory): methodology and results. In: Guidelines for mapping areas at risk of landslides in Europe. 2007; LU: Publications Office.

Trigila A., Iadanza C., Lastoria B., Bussettini M., Barbano A. Dissesto idrogeologico in Italia: pericolosità e indicatori di rischio (En. Geo-Hydrological disruption in Italy: hazards and risk indicators), Edizione 2021, ISPRA, 2021; Rapporti 356/202.

Valkaniotis S, Papathanassiou G, Marinos V, Saroglou C, Zekkos D, Kallimogiannis V, Karantanellis E et al (2022) Landslides triggered by medicane ianos in greece, september 2020: rapid satellite mapping and field survey. Appl Sci. 12:12443. https://doi.org/10.3390/app122312443

Zeng T, Guo Z, Wang L, Jin B, Fayou Wu, Guo R (2023) Tempo-spatial landslide susceptibility assessment from the perspective of human engineering activity. Remote Sens. 15:4111. https://doi.org/10.3390/rs15164111

Publisher's Note

Springer Nature remains neutral with regard to jurisdictional claims in published maps and institutional affiliations.